



# THE UNIVERSITY *of* EDINBURGH

## Edinburgh Research Explorer

### Utility of $^{222}\text{Rn}$ as a passive tracer of subglacial distributed system drainage

**Citation for published version:**

Linhoff, BS, Charette, MA, Nienow, PW, Wadham, JL, Tedstone, AJ & Cowton, T 2017, 'Utility of  $^{222}\text{Rn}$  as a passive tracer of subglacial distributed system drainage' *Earth and Planetary Science Letters*, vol. 462, pp. 180-188. DOI: 10.1016/j.epsl.2016.12.039

**Digital Object Identifier (DOI):**

[10.1016/j.epsl.2016.12.039](https://doi.org/10.1016/j.epsl.2016.12.039)

**Link:**

[Link to publication record in Edinburgh Research Explorer](#)

**Document Version:**

Peer reviewed version

**Published In:**

Earth and Planetary Science Letters

**General rights**

Copyright for the publications made accessible via the Edinburgh Research Explorer is retained by the author(s) and / or other copyright owners and it is a condition of accessing these publications that users recognise and abide by the legal requirements associated with these rights.

**Take down policy**

The University of Edinburgh has made every reasonable effort to ensure that Edinburgh Research Explorer content complies with UK legislation. If you believe that the public display of this file breaches copyright please contact [openaccess@ed.ac.uk](mailto:openaccess@ed.ac.uk) providing details, and we will remove access to the work immediately and investigate your claim.



1 **Utility of  $^{222}\text{Rn}$  as a passive tracer of subglacial distributed system drainage**

2

3 Linhoff, Benjamin S.<sup>1</sup>; Charette, Matthew A.<sup>1</sup>; Nienow, Peter W.<sup>2</sup>; Wadham, Jemma L.<sup>3</sup>;

4 Tedstone, Andrew J.<sup>3</sup>; Cowton, Thomas<sup>2</sup>

5

6 1: Department of Marine Chemistry and Geochemistry, Woods Hole Oceanographic Institution,

7 Woods Hole, Massachusetts, USA

8 2: School of Geosciences, University of Edinburgh, Edinburgh, United Kingdom

9 3: School of Geographical Sciences, University of Bristol, Bristol, United Kingdom

10

11 Corresponding author: Benjamin Linhoff (blinhoff@usgs.gov)

12

13 **Keywords: radon, Greenland, glacier, proglacial river, meltwater.**

14

15 **Abstract**

16 Water flow beneath the Greenland Ice Sheet (GrIS) has been shown to include slow-inefficient

17 (distributed) and fast-efficient (channelized) drainage systems, in response to meltwater delivery

18 to the bed via both moulins and surface lake drainage. This partitioning between channelized and

19 distributed drainage systems is difficult to quantify yet it plays an important role in bulk

20 meltwater chemistry and glacial velocity, and thus subglacial erosion. Radon-222, which is

21 continuously produced via the decay of  $^{226}\text{Ra}$ , accumulates in meltwater that has interacted with

22 rock and sediment. Hence, elevated concentrations of  $^{222}\text{Rn}$  should be indicative of meltwater

23 that has flowed through a distributed drainage system network. In the spring and summer of 2011

24 and 2012, we made hourly  $^{222}\text{Rn}$  measurements in the proglacial river of a large outlet glacier of  
25 the GrIS (Leverett Glacier, SW Greenland). Radon-222 activities were highest in the early melt  
26 season (10-15 dpm  $\text{L}^{-1}$ ), decreasing by a factor of 2-5 (3-5 dpm  $\text{L}^{-1}$ ) following the onset of  
27 widespread surface melt. Using a  $^{222}\text{Rn}$  mass balance model, we estimate that, on average,  
28 greater than 90% of the river  $^{222}\text{Rn}$  was sourced from distributed system meltwater. The  
29 distributed system  $^{222}\text{Rn}$  flux varied on diurnal, weekly, and seasonal time scales with highest  
30 fluxes generally occurring on the falling limb of the hydrograph and during expansion of the  
31 channelized drainage system. Using laboratory based estimates of distributed system  $^{222}\text{Rn}$ , the  
32 distributed system water flux generally ranged between 1-5% of the total proglacial river  
33 discharge for both seasons. This study provides a promising new method for hydrograph  
34 separation in glacial watersheds and for estimating the timing and magnitude of distributed  
35 system fluxes expelled at ice sheet margins.

36

## 37 **1 Introduction**

38 Beneath the ablation zone of the Greenland Ice Sheet (GrIS), meltwater flow paths  
39 influence glacier velocities and bulk meltwater chemistry (Bartholomew et al., 2011a;  
40 Bartholomew et al., 2012; Tedstone et al., 2013; Hawkings et al., 2014). After the onset of spring  
41 melt, the majority of surface derived meltwater travels to the glacier or ice sheet bed through  
42 fractures, crevasses and moulins (Sharp et al., 1993; Das et al., 2008). During the summer, bulk  
43 meltwater is largely composed of two components, channelized drainage and distributed  
44 drainage, which are both derived from snow and ice melt (Tranter et al., 1993; Collins 1979;  
45 Chandler et al., 2013; Cowton et al., 2013). On the time scale of an entire melt season, the major  
46 component is channelized flow, which pertains to meltwater moving efficiently through large

47 basal channels (Röthlisberger, 1972; Nye, 1973). In contrast, distributed drainage refers to  
48 meltwater in slow transit through either cavities that open behind bedrock bumps due to ice  
49 sliding (linked-cavity system; Walder, 1986), a water sheet of near uniform thickness at the ice  
50 bed (Creys and Schoof, 2009), or water flow through permeable subglacial till (Boulton et al.,  
51 2009). Meltwater traveling through distributed systems influences subglacial hydraulic pressure  
52 distribution, channel spacing, basal sliding and bed deformation (Boulton et al., 2009; Rempel,  
53 2009). In general, meltwater in the distributed system tends to have elevated dissolved solid  
54 concentrations, a feature exploited by early attempts at hydrograph separation in glacial  
55 watersheds (Collins, 1979). However, rapid mineral weathering reactions may occur when  
56 sediments traveling through closed, CO<sub>2</sub> limited, distributed systems mix with open-system, low  
57 ionic strength channelized meltwater (Raiswell, 1984; Tranter et al., 1993; Sharp et al., 1993).  
58 Consequently, solute concentrations, often inferred through electrical conductivity (EC)  
59 measurements, cannot unequivocally be used as conservative tracers of distributed system  
60 meltwaters.

61 Radon-222 has been used extensively to examine groundwater-surface water exchange  
62 processes in a wide range of freshwater and marine systems; this is because groundwater <sup>222</sup>Rn  
63 activities are typically highly enriched relative to surface waters due to radioactive decay of  
64 <sup>226</sup>Ra, naturally present in aquifer mineral surfaces (Burnett and Dulaiova, 2003; Cook  
65 et al., 2003; Dulaiova et al., 2008; McCallum et al., 2012). As a relatively soluble, inert noble  
66 gas that does not participate in biogeochemical or weathering reactions once in solution, <sup>222</sup>Rn  
67 (t<sub>1/2</sub> = 3.82 days) can only be added to glacial meltwater in measurable quantities from extensive  
68 water-rock interactions. Hence, by its nature, distributed system meltwater should acquire  
69 significantly higher <sup>222</sup>Rn activities than meltwater that flows through open channels.

70 Discrete  $^{222}\text{Rn}$  measurements in small glacial watersheds have been used to infer the  
71 transition from distributed to channelized drainage (Kies et al., 2010; Bhatia et al., 2011; Kies et  
72 al., 2015). This paper expands upon these earlier studies by examining the utility of long term  
73 continuous  $^{222}\text{Rn}$  measurements in the proglacial river of a large GrIS outlet glacier during the  
74 spring and summer of 2011 and 2012. Using a detailed mass balance modeling approach, we  
75 provide evidence that  $^{222}\text{Rn}$  is a passive tracer of subglacial hydrological routing that can be used  
76 to infer the timing and magnitude of distributed system fluxes. To our knowledge this is the first  
77 time that continuous, high-resolution  $^{222}\text{Rn}$  measurements have been reported from a proglacial  
78 river over the course of a melt season.

79

## 80 **2 Methods**

### 81 *2.1 Study Area*

82 Fieldwork was conducted during the 2011 and 2012 melt seasons at Leverett Glacier, a  
83 large land-terminating glacier on the western margin of the GrIS (67°03'57.81"N, 50°10'01.83";  
84 Figure 1). Its hydrological catchment covers >600 km<sup>2</sup>, reaches an elevation of 1500 m, and  
85 ranges in width from 10-40 km (Bartholomew et al., 2011). Meltwater from the catchment is  
86 channeled through a single large proglacial river (Leverett River); at peak discharge, typical  
87 flows from the river are in the range of 300-400 m<sup>3</sup> s<sup>-1</sup> (Bartholomew et al., 2010; Cowton et al.,  
88 2012). During an exceptional melting period in 2012, the river reached ~800 m<sup>3</sup> s<sup>-1</sup> (Tedstone et  
89 al., 2013). On the south side of Leverett Glacier's snout, the bedrock is a late Achaean (2.5 Ga)  
90 granite (Escher, 1971; Nutman et al., 2010) while the Ikertoq complex (1.85 Ga), composed of  
91 basement gneisses and granites, borders the north side (Henriksen et al., 2000). The proglacial  
92 valley is filled with quaternary sediments composed of weathered materials from afore

93 mentioned rock units (Hindshaw et al., 2014). This suggests that the subglacial lithology is  
94 similar to the bedrock adjacent to the glacier's snout.

95

## 96 2.2 *Discharge, conductivity, suspended sediment, and $^{226}\text{Ra}$ measurements*

97 Proglacial river discharge was measured using continuous water stage monitoring  
98 through a stable bedrock section of the river (Sole et al., 2013; Tedstone et al., 2013). Stage was  
99 converted to discharge using a continuous stage-discharge curve created from repeat Rhodamine  
100 WT and Rhodamine B dye injections throughout both melt seasons; the normalized root mean  
101 squared deviation of the discharge record has been estimated to be  $\pm 10\%$  (Tedstone et al. 2013).  
102 Concurrent measurements of EC and the suspended sediment concentration (SSC) are also  
103 presented here and, for 2011 and 2012 data, in Butler (2014) and Hawkings et al. (2014)  
104 respectively. EC was recorded every five minutes using a Campbell Scientific 247 combined  
105 temperature-EC sensor, and logged using Campbell Scientific CR1000 and CR800 loggers. EC  
106 was calibrated using a KCl solution of known concentration; errors on EC measurements were  
107  $\pm 10\%$  (1-sigma). SSC was estimated from turbidity measurements made with a Partech IR 15C  
108 turbidity probe. Calibration curves were created from discrete suspended sediment samples  
109 collected from the river. Errors on SSC were  $\pm 6\%$  (1-sigma). Dissolved  $^{226}\text{Ra}$  was measured  
110 throughout the 2011 and 2012 field seasons using methods described by Charette et al. (2001).  
111 Briefly,  $\sim 200$  L river samples were filtered through a column packed with  $\text{MnO}_2$  impregnated  
112 fiber. The fiber was ashed, packed in a sealed plastic vial, and counted for 2-3 days on a well-  
113 type germanium gamma detector (Canberra) calibrated using a NIST  $^{226}\text{Ra}$  standard prepared in  
114 the same manner as the samples.

115

116 2.3 *Measuring radon in the proglacial river*

117 Radon-222 was measured in the Leverett Glacier proglacial river during 2011 (May 8-  
118 August 5) and 2012 (May 12-July 28). Continuous (hourly) measurements were made using a  
119 RAD7 (DurrIDGE Inc.) radon-in-air monitor in series with a desiccant chamber and a RAD7  
120 water probe, a submersible air-filled gas-permeable membrane coil made from Accruel® tubing  
121 (henceforth the term “water probe” will refer to the <sup>222</sup>Rn extraction unit). River water <sup>222</sup>Rn  
122 equilibrates with air in the membrane coil through passive diffusion; the air is continuously  
123 circulated in a closed loop through the RAD7 radon-in-air monitor system (Hofmann et al., 2011;  
124 Schubert et al., 2012). Radon-in-air activities were then converted to radon-in-water activity via  
125 the temperature dependent air–water partition coefficient as described by Schubert et al. (2012).  
126 The water probe was deployed on the northern bank of the river as close to the glacier’s terminus  
127 as possible (0-1 km) to minimize potential evasion of <sup>222</sup>Rn from the river to the atmosphere  
128 (Supplementary Material). Rising river stage required that we periodically moved the water  
129 probe downstream to a more stable riverbank. There was no observed decrease in effectiveness  
130 of the water probe during long term deployment (Supplementary Material). Typical 1-sigma  
131 counting errors for the water probe <sup>222</sup>Rn activities were ±5-20%. Discrete <sup>222</sup>Rn samples were  
132 collected upstream of the water probe at the ice sheet terminus in 250 mL bottles and analyzed  
133 using a RAD7 plus Rad-H<sub>2</sub>O attachment on a regular basis (Figure S1; Supplementary Material).  
134 These discrete <sup>222</sup>Rn samples agree within the counting errors of the corresponding continuous  
135 <sup>222</sup>Rn measurements (Figure S1; Supplementary Material).

136 Measurements of <sup>222</sup>Rn via the water probe system may lag actual aqueous <sup>222</sup>Rn due to  
137 the time required to equilibrate <sup>222</sup>Rn across the gas-permeable membrane (Schubert et al., 2012).  
138 To assess the magnitude of this offset, we analyzed field equilibration times during instrument

139 startup and performed laboratory experiments to estimate the water probe's response time to  
140 changes in  $^{222}\text{Rn}$  activity. Key factors that control the equilibration time include the air volume in  
141 the system (RAD7 unit, tubing, desiccant and membrane coil), the membrane coil surface area,  
142 and the  $^{222}\text{Rn}$  activity gradient across the membrane water/air interface (Schubert et al., 2012).  
143 The equilibration time can be minimized when the air volume of the system is low (i.e. using less  
144 tubing between RAD7 and membrane), the membrane interface area is maximized (i.e.  
145 lengthening the membrane tubing), and the water/air  $^{222}\text{Rn}$  activity gradient across the membrane  
146 coil is large. The  $^{222}\text{Rn}$  activity gradient at the membrane water/air interface has by far the largest  
147 effect on the equilibration and response time of the water probe; in stagnant water the response  
148 time is on the order of several hours (Hofmann et al., 2011; Schubert et al., 2012). In a flowing  
149 river, the activity gradient at the water/air interface is close to 100% such that the response time  
150 can be reduced to <1 hour, similar to results obtained using a spray chamber equilibrator such as  
151 the RAD-Aqua (DurrIDGE Inc.; Schubert et al., 2012). In our case, the equilibration time of the  
152 water probe in the proglacial river was determined to be no greater than 2 hours based on  
153 laboratory experiments and less than 1 hour in field observations. A detailed description of these  
154 tests and associated results is presented in the Supplementary Material.

155

#### 156 2.4 $^{222}\text{Rn}$ in subglacial distributed systems and sediment properties

157 Because we were unable to obtain *in-situ* distributed system samples from beneath the ice  
158 sheet, we estimated  $^{222}\text{Rn}$  in this environment via laboratory-based equilibration experiments  
159 (Corbett et al., 1998; Dulaiova et al., 2008) using sediments discharged from the subglacial  
160 environment. For these tests, four separate aliquots of sediment (50 g) from the proglacial river  
161 were incubated with Ra-free water in a sealed 1 L high-density polyethylene bottle for greater



162 than five half-lives (>20 days). Samples were flushed into a cold trap and scintillation cells using  
163 helium and analyzed in triplicate on alpha scintillation counters (Corbett et al., 1998). Wet  
164 sediment  $^{222}\text{Rn}$  activities in  $\text{dpm g}^{-1}$  were converted to pore water  $^{222}\text{Rn}$  activities ( $\text{dpm L}^{-1}$ ) using  
165 wet bulk densities and porosities (Supplementary Material).

166 Radon-222 diffusion from sediments in subglacial channels was another potential source  
167 of  $^{222}\text{Rn}$  beneath the GrIS. We employed a laboratory method described by Chanyotha et al.  
168 (2014) to quantify the diffusive flux. Briefly, 100 g of wet subglacial sediment and 500 mL of  
169  $^{222}\text{Rn}$ -free water were sealed inside a gas tight reaction flask connected in a closed loop with a  
170 RAD7. Air was pumped through a gas diffusion stone immersed in the water phase using the  
171 built in RAD7 pump, then through the desiccant, and back to the radon analyzer where the  
172 activity was measured and recorded. While gas leakage is not an issue for routine measurements,  
173 a known small leak within the internal air pump of the RAD7 was corrected during the multi-day  
174 experiment according to the approach described in Chanyotha et al. (2014). The diffusive flux  
175 was determined from the near-linear slope of  $^{222}\text{Rn}$  activity in the reaction flask versus time over  
176 the first several hours of the experiment. Slope uncertainty was used to estimate the uncertainty  
177 of the diffusive flux.

178 Leakage is an issue for this approach, not necessarily from diffusion through the walls of  
179 the plastic bottle but from a known small leak in the internal air pump of the RAD7 as described  
180 in Chanyotha et al. (2014). This is not an issue for routine measurements with the RAD7, but  
181 needs to be corrected for in the multi-day sediment equilibration method. The data has been leak  
182 corrected according to the approach described in Chanyotha et al. (2014)

183

184 **3 Results**

185 *3.1 Discharge*

186 Warmer average air temperatures resulted in nearly twice as much annual discharge in  
187 2012 as in 2011, corresponding to  $\sim 2.4$  and  $1.4 \text{ km}^3$ , respectively within the Leverett Glacier  
188 catchment (Figure 2). Average flows of the proglacial river in the summer were  $\sim 200 \text{ m}^3 \text{ s}^{-1}$  in  
189 2011 (Sole et al., 2013) and  $\sim 400 \text{ m}^3 \text{ s}^{-1}$  in 2012 (Tedstone et al., 2013). In 2012, the largest  
190 melting event since at least 1889, as indicated by ice cores at the Summit Station, occurred on  
191 July 12<sup>th</sup> (day 194) when over 98% of the surface of the GrIS experienced melting (Nghiem et  
192 al., 2012). During this period, river discharge reached  $\sim 800 \text{ m}^3 \text{ s}^{-1}$  (Tedstone et al., 2013), almost  
193 three times larger than maximum discharge in 2011 (Figure 2; Sole et al., 2013). Furthermore, in  
194 2011 the river was largely ice-covered until day 160, while in 2012 the river was ice free from  
195 the start of sampling (day 133) onward.

196

197 *3.2 EC and SSC*

198 We used EC as a proxy for the concentration of dissolved solutes in the proglacial river.  
199 During both 2011 and 2012, EC was elevated in the early season ( $60\text{-}100 \mu\text{S cm}^{-1}$ ) and decreased  
200 to  $10\text{-}20 \mu\text{S cm}^{-1}$  with increasing river discharge (Figure 2; Butler, 2014; Hawkings et al., 2014).  
201 These results are consistent with the EC range reported in 2009 (Bartholomew et al., 2011).  
202 Butler (2014) and Hawkings et al. (2014) observed diurnal variations in EC through much of the  
203 2011 and 2012 seasons, which in general were inverse to river discharge. During both seasons,  
204 peaks in EC punctuated the record.

205 The SSC varied between  $1\text{-}7 \text{ g L}^{-1}$  in 2011 (Butler, 2014) and  $1\text{-}4 \text{ g L}^{-1}$  in 2012  
206 (Hawkings et al., 2014); these concentrations were similar to values reported for 2009 and 2010

207 (Cowton et al., 2012). Like EC, diurnal variations in SSC occurred throughout much of the 2011  
208 and 2012 melt seasons, however, these diurnal variations in SSC generally increased with rising  
209 river discharge. In 2012, peaks in SSC and EC generally occurred simultaneously (Figure 2,  
210 dashed boxes) as noted by Hawkings et al. (2014) and in line with observations in 2009  
211 (Bartholomew et al, 2009). In 2011, SSC and EC peaks were largely decoupled (Figure 2).

212

### 213 3.3 *Radon-222 in the Proglacial River*

214 In both 2011 and 2012, the highest  $^{222}\text{Rn}$  activities were observed in the early season and  
215 generally decreased with increasing river discharge (Figure 2). In 2011, typical  $^{222}\text{Rn}$  activities in  
216 the early season (days 132-160) were between 10-15 dpm L<sup>-1</sup>. Following day 170, activities were  
217 generally between 2-5 dpm L<sup>-1</sup>. In 2012, higher  $^{222}\text{Rn}$  activities were observed in the early  
218 season, typically between 5-18 dpm L<sup>-1</sup>, falling to between 2-10 dpm L<sup>-1</sup> after day 150. In a small  
219 proglacial river ~100 km north of our field site, Bhatia et al. (2011) reported significantly higher  
220  $^{222}\text{Rn}$  activities (25-76 dpm L<sup>-1</sup>), though peak river discharge rates (~2 m<sup>3</sup> s<sup>-1</sup>) were orders of  
221 magnitude lower than at Leverett Glacier. Regardless, activities measured in this study and in  
222 Bhatia et al. (2011) are much higher than those generally observed in non-glaciated river  
223 catchments. For example, both Cook et al. (2003) and McCallum et al. (2012) report maximum  
224  $^{222}\text{Rn}$  activities of ~1 dpm L<sup>-1</sup> in tropical and temperate rivers.

225 Significant peaks in  $^{222}\text{Rn}$  are highlighted in Figure 2 by grey shaded boxes. In 2011,  
226  $^{222}\text{Rn}$  peaked at ~75 dpm L<sup>-1</sup> in the early season (days 148-150); during this time, the river was  
227 ice covered and a small upwelling spring appeared at the glacier portal through which nearly all  
228 river discharge originated. A second large peak (days 190-200) was observed in  $^{222}\text{Rn}$  when  
229 activities climbed to ~15 dpm L<sup>-1</sup> from a pre-peak baseline of 3 dpm L<sup>-1</sup> over a ~5 day period

230 (Figure 2). In 2012,  $^{222}\text{Rn}$  peaks occurred regularly, approximately once every 8-10 days  
231 throughout the season (Figure 2). Radon-222 peaks in 2012 generally increased on the falling  
232 limb or inflection point of the hydrograph and decreased when river discharge rose (Figure 2).  
233 This general relationship between discharge and  $^{222}\text{Rn}$  was not observed in 2011. In both field  
234 seasons,  $^{222}\text{Rn}$  did not correlate with SSC or EC.

235

### 236 3.4 Radon activity in distributed system meltwater

237 Laboratory derived distributed system  $^{222}\text{Rn}$  activities ( $Rn_{dis}$ ) were estimated using the  
238  $^{222}\text{Rn}$  activity of porewater in sediments collected from the proglacial river (Section 2.4) and  
239 sediment properties (Corbett et al., 1998) including bulk density ( $\rho_B$ ) and porosity ( $\phi$ ;  
240 Supplementary Material). Wet sediment  $^{222}\text{Rn}$  activities ( $Rn_{sed}$ ) were 0.064-0.093 dpm g<sup>-1</sup>  
241 (avg=0.076 dpm g<sup>-1</sup>, n=4).  $\rho_B$  and  $\phi$  were identical for the three glacial river sediment samples  
242 analyzed and were 1.7 g cm<sup>-3</sup> and 0.37 respectively. Our results are consistent with those of Dow  
243 et al. (2013), who estimated subglacial sediment  $\phi$  in the Leverett Glacier catchment between  
244 0.3-0.4. Using Equation 1 and assuming that subglacial sediment  $\phi$  varied between 0.3-0.4, that  
245  $Rn_{sed}$  was between 0.064-0.093 dpm g<sup>-1</sup>, and that  $\rho_B=1.7$  g cm<sup>-3</sup>,  $Rn_{dis}$  would be expected to span  
246 from 270-530 dpm L<sup>-1</sup>.

247

$$248 \quad Rn_{dis} = \frac{Rn_{sed} \times \rho_B}{\phi} \times 1000 (g L^{-1}) \quad (1)$$

249

250 These values are lower than laboratory derived pore water  $^{222}\text{Rn}$  activities in proglacial  
251 sediments reported by Bhatia et al. (2011), which were between 1285-3045 dpm L<sup>-1</sup>. A number  
252 of factors could explain the difference between the two sites: including sediment grain size

253 (higher surface area/volume), degree of weathering (affects sediment  $^{226}\text{Ra}$  parent activities), or  
254  $^{238}\text{U}$  content of the sediment (Dulaiova et al., 2008).

255

## 256 **4 Discussion**

### 257 *4.1 Radon-222 sources and sinks*

258 Radon-222 has been used as a tracer of sediment pore water-surface water exchange  
259 processes in a diverse range of environmental systems including rivers (McCallum et al., 2012),  
260 the coastal ocean (Burnett and Dulaiova, 2003; Dulaiova et al., 2008), and in small glacier  
261 catchments (Kies et al., 2010; Bhatia et al., 2011; Kies et al., 2015). In the following discussion,  
262 we explore the utility of  $^{222}\text{Rn}$  in tracing and quantifying meltwater fluxes from the subglacial  
263 distributed system at a large Greenland outlet glacier, Leverett Glacier. There are a number of  
264 sources and sinks capable of modulating  $^{222}\text{Rn}$  activities in a proglacial river. We use a mass  
265 balance approach, similar to those employed in studies of submarine groundwater discharge to  
266 the coastal ocean (Burnett and Dulaiova, 2003; Dulaiova et al., 2008), in order to quantify the  
267 sources and sinks for  $^{222}\text{Rn}$  in the proglacial river (Figure 3):

268

$$269 \quad J_{riv} = J_{dis} + J_{cha} + P_{SSL} + \lambda^{226}\text{Ra} - J_{atm} - \lambda^{222}\text{Rn} \quad (2)$$

270

271 Sources of  $^{222}\text{Rn}$  include production from  $^{226}\text{Ra}$  associated with suspended sediments ( $P_{SSL}$ ),  
272 production of  $^{222}\text{Rn}$  through the decay of dissolved  $^{226}\text{Ra}$  ( $\lambda^{226}\text{Ra}$  where  $\lambda$  is the decay constant  
273 for  $^{222}\text{Rn}$ ),  $^{222}\text{Rn}$  diffusion through subglacial channel sediments ( $J_{cha}$ ), and distributed system  
274 meltwater ( $J_{dis}$ ). Radon-222 sinks include radioactive decay ( $\lambda^{222}\text{Rn}$ ) and atmospheric evasion  
275 across the water/air interface ( $J_{atm}$ ). Finally,  $J_{riv}$  is the  $^{222}\text{Rn}$  flux ( $\text{dpm s}^{-1}$ ) exported to the

276 glacier's front via the proglacial river and is derived by combining our continuous  $^{222}\text{Rn}$   
277 measurements ( $\text{dpm m}^{-3}$ ) with the discharge record ( $\text{m}^3 \text{s}^{-1}$ ). All source/sink terms can be directly  
278 evaluated except for  $J_{dis}$ ; hence we use the "flux by difference" approach (Charette et al., 2008),  
279 which assumes that the unaccounted for  $^{222}\text{Rn}$  in the mass balance model must be due to  
280 distributed system meltwater ( $J_{dis}$ ). We discuss and evaluate each source and sink term for  
281 Equation 2 in the following sections. To provide context for the various source and sink terms  
282 below, note that  $J_{riv}$  ranged from  $3.4\text{-}4.2 \times 10^6 \text{ dpm s}^{-1}$  and  $7.2 \times 10^3\text{-}3.4 \times 10^6 \text{ dpm s}^{-1}$ , for 2011 and  
283 2012, respectively.

284

#### 285 4.1.1 *Suspended sediment $^{226}\text{Ra}$ ( $P_{SSL}$ )*

286 Suspended sediments are a potential source of  $^{222}\text{Rn}$  to the river through decay of  
287 sediment bound  $^{226}\text{Ra}$ . From the laboratory equilibration experiments described above (Section  
288 2.4) we determined that the surface-bound  $^{222}\text{Rn}$  activity of sediments at secular equilibrium is  
289  $0.076 \text{ dpm g}^{-1}$  (Section 3.4). To calculate  $P_{SSL}$ , we first assume that suspended sediments could  
290 produce  $^{222}\text{Rn}$  for 1-18 hours, the range of transit times observed for surface meltwater traveling  
291 through channelized drainage in the Leverett Glacier catchment (Chandler et al., 2013; Chandler  
292 et al., submitted). Coupling this result with SSC measurements, and assuming that bedload  
293 contributed an additional 30-60% of sediment (Cowton et al., 2012), we estimated the upper and  
294 lower bounds of the contribution from  $P_{SSL}$  to  $J_{riv}$ . Over the course of each melt season,  $P_{SSL}$   
295 supplied between  $\sim 100$  and  $2.1 \times 10^4 \text{ dpm s}^{-1}$   $^{222}\text{Rn}$  in 2012 and  $\sim 100$  and  $2.4 \times 10^4 \text{ dpm s}^{-1}$   $^{222}\text{Rn}$   
296 in 2011. On average, the upper limit of our  $P_{SSL}$  estimate contributed on average  $\sim 1\%$  of  $J_{riv}$  in  
297 2011 and 2012, respectively (Figure 4).

298

299 4.1.2 Dissolved  $^{226}\text{Ra}$  ( $\lambda^{226}\text{Ra}$ )

300 The proglacial river also carried dissolved  $^{226}\text{Ra}$ , which could have supported  $^{222}\text{Rn}$  via  
301 its decay. We observed  $^{226}\text{Ra}$  activities of 0.02-0.09 dpm L<sup>-1</sup> (avg 0.04 dpm L<sup>-1</sup>, n=21) in the  
302 proglacial river, with higher values in the early season and lower values in the late season. To  
303 solve Equation 2 for  $J_{dis}$ , we used the average  $^{226}\text{Ra}$  activity measured in the proglacial river.  
304 Based on these results,  $^{226}\text{Ra}$  decay supplies  $\sim 400$  dpm s<sup>-1</sup> when river discharge was 10 m<sup>3</sup> s<sup>-1</sup>  
305 and up to  $3.2 \times 10^4$  dpm s<sup>-1</sup> during the maximum river discharge observed in 2012. On average  
306 during the 2011 and 2012 field seasons, dissolved  $^{226}\text{Ra}$  supplies  $\sim 1\%$  of  $J_{riv}$  (Figure 4).

307

308 4.1.3 Diffusive flux of  $^{222}\text{Rn}$  in channels ( $J_{cha}$ )

309 The diffusive flux of  $^{222}\text{Rn}$  from channel floor sediments (subglacial or proglacial) is a  
310 potential source of  $^{222}\text{Rn}$ , particularly after the onset of widespread melting across the catchment  
311 and development of a channelized system. Our laboratory sediment diffusion experiment yielded  
312 a diffusive flux of  $0.006 \pm 0.002$  dpm m<sup>-2</sup> s<sup>-1</sup>  $^{222}\text{Rn}$  from glacial sediments. We use this result and  
313 an estimate of channel floor area during peak river discharge to quantify the potential upper limit  
314 of  $J_{cha}$ . To calculate channel floor area, we assume that all discharge moved through semi-  
315 circular channels, that channels extended to 41 km from the ice margin (Chandler et al., 2013),  
316 that the average number of channels per km catchment width was four (Schoof, 2010; Werder et  
317 al., 2013), and that channel density linearly tapered to zero between the ice sheet margin and 41  
318 km. Furthermore, we assumed that catchment width averaged 40 km (Bartholomew et al., 2011)  
319 and that water moved through channels at 3 m s<sup>-1</sup> (Cowton et al., 2013). Using these constraints,  
320 we calculated a channel floor area of 2.75 km<sup>2</sup> during peak river discharge in 2012 and 1.5 km<sup>2</sup>  
321 during peak river discharge in 2011. This estimate amounts to 0.3-0.5% of the glacier's

322 catchment area, which is consistent with models of the channelized system (Schoof, 2010;  
323 Werder et al., 2013). Using these estimates of channel floor area,  $J_{cha}$  supplied  $\sim 6 \times 10^3 - 1.2 \times 10^4$   
324  $\text{dpm s}^{-1}$   $^{222}\text{Rn}$  in 2011 and  $1.1 \times 10^4 - 2.2 \times 10^4$   $\text{dpm s}^{-1}$   $^{222}\text{Rn}$  in 2012. Finally, we assume that  $J_{cha}$  is  
325 only important after river discharge surpasses  $100 \text{ m}^3 \text{ s}^{-1}$  as before this time the channelized  
326 system is undeveloped (Cowton et al., 2013), and hence,  $^{222}\text{Rn}$  diffusion through channel floors  
327 is negligible. Based on these estimates,  $J_{cha}$  could account for no more than  $<1-10\%$  of  $J_{riv}$  in  
328 2011 and 2012 (Figure 4).

329

#### 330 4.1.4 Gas exchange ( $J_{atm}$ )

331 The degassing of  $^{222}\text{Rn}$  out of water is a function of molecular diffusion produced by the  
332 activity gradient at the water/air interface as well as turbulent transfer, which is governed by  
333 physical processes such as wind speed, current velocity, and topography.  $J_{atm}$ , which we define  
334 as the area-normalized flux of  $^{222}\text{Rn}$  across the river/air boundary, can be written as:

335

$$336 J_{atm} = k(C_w - \alpha C_{atm}) \quad (3)$$

337

338 where  $C_w$  is the  $^{222}\text{Rn}$  activity of water,  $C_{atm}$  is the  $^{222}\text{Rn}$  activity in air (assumed here to be  
339 negligible relative to the water activity),  $\alpha$  is Ostwald's solubility constant and  $k$  is the gas  
340 transfer velocity. The gas transfer velocity is dependent on kinematic viscosity, molecular  
341 diffusion, and turbulence and is determined based on empirical relationships observed in  
342 different environments for different gases. Borges et al. (2004) suggested that the gas transfer  
343 velocity  $k$  should be in the range of  $3-7 \text{ cm hr}^{-1}$  while Dulaiova and Burnett (2006) calculated a  
344 gas transfer velocity for  $^{222}\text{Rn}$  up to  $10 \text{ cm hr}^{-1}$  in moving water and high winds.



345           Because of occasional strong winds and a river current of  $\sim 1\text{-}3\text{ m s}^{-1}$  (Cowton et al.,  
346 2013), we chose a constant, upper limit  $k$  of  $12\text{ cm hr}^{-1}$  for the duration of the time series. With  
347 these assumptions,  $J_{atm}$  varied between  $<0.01\text{-}0.7\text{ dpm m}^{-2}\text{ s}^{-1}$  in 2011 and  $0.03\text{-}0.6\text{ dpm m}^{-2}\text{ s}^{-1}$  in  
348 2012. Scaling these area normalized  $J_{atm}$  values to total  $J_{atm}$  requires an estimate of river surface  
349 area ( $1100\text{-}6000\text{ m}^2$ ) between the ice terminus and the sampling site. From this surface area we  
350 determined that  $J_{atm}$  was in the range of  $800\text{-}4,000\text{ dpm s}^{-1}\text{ }^{222}\text{Rn}$ , which was  $<1\%$  of  $J_{riv}$  on  
351 average. The negligible effect of gas loss suggested by these calculations is supported by discrete  
352  $^{222}\text{Rn}$  samples collected at the glacier's terminus, which were within error of the continuous  
353 measurements made 1 km downstream (Figure S1; Supplementary Material).

354           These estimates do not account for any potential loss of  $^{222}\text{Rn}$  into the headspace of  
355 subglacial air-filled cavities. However, if these environments are largely closed systems,  $^{222}\text{Rn}$   
356 build up in the headspace would reduce the water-air concentration gradient and therefore  
357 minimize the  $^{222}\text{Rn}$  loss from the water phase. While there is evidence for open system channels  
358 at the ice bed within several km from the ice margin (Chandler et al., 2013), subglacial gas loss  
359 is likely much smaller than in the proglacial river. Air-filled subglacial channels far from the ice  
360 sheet margin will only exist during the falling limb of the hydrograph following substantial  
361 surface meltwater inputs and channel expansion. These cavities will close within hours to days of  
362 opening because of glacial creep (Meierbachtol et al., 2013). If large quantities of  $^{222}\text{Rn}$  were lost  
363 to air-filled cavities, then  $^{222}\text{Rn}$  activities would decrease on the falling limb of the hydrograph  
364 yet we generally observed the opposite trend in 2012 (Figures 2). Based on our calculations and  
365 field measurements (Supplementary Material), we determined that  $J_{atm}$  was negligible in our  
366 calculation of  $J_{dis}$ .

367

368 4.1.5 *Radon-222 decay ( $\lambda^{222}\text{Rn}$ )*

369 When distributed system meltwater discharges into the channelized system far from the  
370 ice margin, some fraction of  $^{222}\text{Rn}$  will decay before reaching the ice terminus. For example,  
371 during a typical 7 hour transit through the channelized system of Leverett Glacier in July  
372 (Cowton et al., 2013), ~5% of unsupported  $^{222}\text{Rn}$  will decay. During the early melt season, when  
373 the snow line is at a low elevation and river discharge is  $<10 \text{ m}^3 \text{ s}^{-1}$ , meltwater transit times in  
374 channelized drainage are likely no more than 3 hours as water takes a more direct route to the  
375 margin (Chandler et al., 2013; Cowton et al., 2013). In this case, 2% of the unsupported  $^{222}\text{Rn}$   
376 decays in the channelized system before reaching the ice margin. By the peak melt season, tracer  
377 experiments indicate that transit times in the channelized drainage system are 10-24 hours  
378 (Chandler et al., (submitted) since the catchment extends upwards of ~80 km from the margin  
379 and subglacial flow paths are more convoluted. As the location of these experiments was likely  
380 near the upper limit of channelized drainage in the catchment (Chandler et al., 2013), we assume  
381 nearly all meltwater traveling via channelized drainage reaches the ice sheet margin in  $<24$   
382 hours. Hence for our model, we assume meltwater moving through the channelized system has a  
383 transit time between 1 and 24 hours representing a  $<1-17\%$  loss of  $^{222}\text{Rn}$ .

384

385 4.2 *Quantifying the distributed system flux*

386 After rearranging Equation 2, we solved for the upper and lower bounds of  $J_{dis}$  (Figure 5).

387

388 
$$J_{dis} = J_{riv} - J_{cha} - P_{SSL} - \lambda^{226}\text{Ra} + \lambda^{222}\text{Rn} \quad (4)$$

389

390 To calculate the likely range of  $J_{dis}$ , we propagated the uncertainty of each  $^{222}\text{Rn}$  source and sink.  
391 The largest source of uncertainty in  $J_{dis}$  came from the  $^{222}\text{Rn}$  and river discharge measurements  
392 used to calculate  $J_{riv}$ .

393 With the exception of days 200-202 in 2011 when  $J_{riv}$  dropped to near zero, non-  
394 distributed system  $^{222}\text{Rn}$  sources cannot account for the vast majority of  $J_{riv}$  (Figure 4), we  
395 conclude that  $J_{dis}$  must contribute the bulk of the  $^{222}\text{Rn}$  flux in the proglacial river. Furthermore,  
396  $^{222}\text{Rn}$  decay during subglacial transit through the channelized system ( $\lambda^{222}\text{Rn}$ ) and gas loss to the  
397 atmosphere ( $J_{atm}$ ), did not significantly impact the timing or flux of  $J_{riv}$ . Given that  $J_{dis}$  dominates  
398 the  $^{222}\text{Rn}$  mass balance for the Leverett Glacier proglacial river, we conclude that  $^{222}\text{Rn}$  can be  
399 used as a passive tracer of distributed system flows to the ice margin at this field site. This  
400 approach should be applicable to other settings, though an essential requirement is subglacial  
401 hydrological systems that discharge into a single proglacial river, which permits the  
402 quantification of  $J_{riv}$ , the main term in the model.

403 The distributed system meltwater flux ( $Q_{dis}$ ) can be calculated if  $J_{dis}$  and the  $^{222}\text{Rn}$  activity  
404 of distributed system meltwater ( $Rn_{dis}$ ) are known:

405

$$406 \quad Q_{dis} = J_{dis} / Rn_{dis} \quad (5)$$

407

408 This approach assumes that distributed system meltwaters originate from material similar  
409 to the proglacial sediments we used to estimate  $Rn_{dis}$  (Sections 2.4 and 3.4), and that the transit  
410 time of distributed system meltwaters are >20 days (Niu et al., 2015). If the transit time is  
411 shorter,  $Rn_{dis}$  would decrease and the  $Q_{dis}$  fluxes below would increase proportionately.

412 If the  $^{222}\text{Rn}$  activities in distributed system sediments are 270-530 dpm  $\text{L}^{-1}$  (Sections 2.4  
413 and 3.4), then  $Q_{dis}$  would vary between <0.1 to 17  $\text{m}^3 \text{s}^{-1}$  and <0.1 to 14  $\text{m}^3 \text{s}^{-1}$  over the course of  
414 the 2011 and 2012 melt seasons, respectively. As a fraction of total river discharge in 2011,  $Q_{dis}$   
415 peaked at ~22% in the early season when river discharge was ~1  $\text{m}^3 \text{s}^{-1}$  and reached a minimum  
416 of <0.1% between days 202-204. In 2012,  $Q_{dis}$  was between 3-5% (0.1-0.5  $\text{m}^3 \text{s}^{-1}$ ) of total river  
417 flow in the early season (days 130-150) and 1-4% (0.1-33  $\text{m}^3 \text{s}^{-1}$ ) following day 150. The  
418 weighted mean of  $Q_{dis}$  relative to total river discharge was between 1-2.4% (0.35-8.5  $\text{m}^3 \text{s}^{-1}$ ) in  
419 2011 and 0.7-1.6% (<1-12.8  $\text{m}^3 \text{s}^{-1}$ ) in 2012. However, since we were not able to obtain samples  
420 of distributed system water directly via borehole sampling (Tranter et al., 1997; Andrews et al.,  
421 2014), these estimates of  $Q_{dis}$  carry significant uncertainty; therefore, we will use  $J_{dis}$  for  
422 determining the timing and relative magnitude of distributed system fluxes.

423

#### 424 4.3 *Seasonal and interannual variability in the distributed system flux*

425 Channels at the ice sheet bed are zones of low-pressure relative to the surrounding  
426 distributed system (Röthlisberger, 1969) and generally act to scavenge distributed system  
427 meltwater (Boulton et al., 2009). However, during large surface runoff events, such as  
428 supraglacial lake drainages or periods of rapid warming, channels may be overwhelmed forcing  
429 water into the distributed system (Bartholomew et al., 2012; Gulley et al., 2012). Once surface  
430 meltwater runoff decreases, water pressure in channels falls and the flux of distributed system  
431 drainage to the ice sheet margin surges (Hubbard et al., 1995; Boulton et al., 2009). This process  
432 has been hypothesized to result in more connectivity between channelized and distributed  
433 systems causing an overall increase in the spatial extent of subglacial drainage (Andrews et al.,  
434 2014). This in turn may lead to less water volume at the ice sheet bed and could explain observed

435 mid-late summer slowing of land-terminating sections of the GrIS (Sole et al., 2013). Hence, the  
436 mechanisms that control the characteristics of distributed system drainage likely play a key roll  
437 in modulating the speed of GrIS outlet glaciers, especially because distributed system networks  
438 make up by far the largest portion of the ice sheet bed area.

439 In 2011, the largest multiday peak in  $J_{dis}$  (Figure 5) (days 190-200) occurred during the  
440 onset of melting and ice acceleration (Sole et al., 2013) at high elevations (>1400 m) within the  
441 catchment, and the expansion of the channelized system to at least 40 km from the ice sheet  
442 margin (Chandler et al., 2013). During the 2012 time series, there were four major multiday  
443 peaks in  $J_{dis}$  (Figure 5). The largest 2012 peak occurred on the falling limb of the hydrograph of  
444 the widely publicized extreme melting event (Nghiem et al., 2012) during which river discharge  
445 reached  $\sim 800 \text{ m}^3 \text{ s}^{-1}$  (day 196; Figure 5). These results provide direct evidence that drainage of  
446 distributed regions follows periods of channelized system expansion due to rapid increases in  
447 surface meltwater runoff. Following the largest peaks in  $J_{dis}$  in 2011 and 2012, significant diurnal  
448 variations were observed in  $J_{dis}$  (days 205-210 in 2011 and days 199-205 in 2012; Figure 6).  
449 These daily cycles in  $J_{dis}$  suggest a high degree of connectivity between the distributed and  
450 channelized systems with increases in flux from the distributed on the falling limb of the  
451 hydrograph when subglacial water pressure subsides (Figure 6).

452 Bartholomew et al. (2011) and Butler (2014) found evidence that SSC/EC peaks at  
453 Leverett Glacier are triggered by supraglacial lake drainage events. These events likely increase  
454 the connectivity of the channelized system (Bartholomew et al., 2011a), and may lead to the  
455 expulsion of distributed system meltwater. In general, peaks in  $J_{dis}$  were not correlated with  
456 SSC/EC peaks, nor did peaks in SSC/EC lead to enhanced  $^{222}\text{Rn}$  concentrations (Figure 2). Lake  
457 drainage events clearly increase the suspended sediment load which may lead to post mixing

458 solute acquisition reactions, causing meltwaters to rapidly acquire dissolved solutes (Raiswell,  
459 1984; Tranter et al., 1993). Conversely,  $^{222}\text{Rn}$  equilibrium in the distributed system will likely be  
460 reached long before subglacial meltwaters become saturated with respect to weathering minerals.  
461 Hence, we would expect more variation in solute concentrations (EC) in the distributed system  
462 than  $^{222}\text{Rn}$  activities. Consequently, lake drainage events could produce the observed SSC/EC  
463 peaks without a corresponding  $J_{dis}$  peak if they act to flush small volumes of distributed system  
464 meltwater with high solute concentrations to the ice sheet margin.

465

## 466 **5 Conclusions**

467 Using a mass balance model for  $^{222}\text{Rn}$  in a large glacial catchment of the GrIS, we found  
468 that on average, >90% of the  $^{222}\text{Rn}$  in the proglacial river is sourced from the subglacial  
469 distributed system. Hence, at Leverett Glacier,  $^{222}\text{Rn}$  acts as a conservative, passive tracer of  
470 distributed system meltwater fluxes. These fluxes varied on diurnal, seasonal, and interannual  
471 time scales. Based on  $^{222}\text{Rn}$  measurements, large peaks in distributed system drainage appear to  
472 be initiated by the expansion of the channelized system into presumably distributed regions of  
473 the ice sheet bed and by rapid increases in supraglacial meltwater runoff. During a large multiday  
474  $J_{dis}$  peak in 2011 (days 190-200; Figure 5),  $\text{SF}_6$  tracer experiments (Chandler et al., 2013) and ice  
475 acceleration (Sole et al., 2013) suggested the channelized network expanded coincident with the  
476  $J_{dis}$  peak. In 2012, four major multiday  $J_{dis}$  peaks were observed (Figure 5), the biggest of which  
477 occurred on the falling limb of the hydrograph during the largest surface meltwater runoff event  
478 observed in Greenland since at least 1889 (days 196; Nghiem et al., 2012). These results imply  
479 that rapid warming events, which initially cause short term glacial acceleration (Tedstone et al.,  
480 2013), may lead to enhanced distributed system drainage, a process which could lessen the total

481 water volume at the ice sheet bed and ultimately, explain the observed mid-summer ice sheet  
482 slowing at Leverett Glacier (Sole et al., 2013; Tedstone et al., 2013). Following the largest peaks  
483 in  $J_{dis}$  in 2011 and 2012, significant diurnal variations were observed in  $J_{dis}$ , indicative of a  
484 highly connected distributed system whereby the distributed system water flux substantially  
485 increases at night when channelized system water pressure subsides.

486         Based on our laboratory-based sediment equilibration measurements of  $^{222}\text{Rn}$  activities in  
487 distributed system fluids, we estimate that distributed system meltwater fluxes vary seasonally  
488 and are on the order of 1-5% of river discharge. The weighted mean  $Q_{dis}$  relative to total river  
489 discharge was between 1-2.4% in 2011 and 0.7-1.6% in 2012. Future studies should endeavor to  
490 collect samples for  $^{222}\text{Rn}$  analysis directly from distributed and channelized systems so as to  
491 better constrain  $Q_{dis}$ . Furthermore, utilizing continuous  $^{222}\text{Rn}$  measurements provides a practical  
492 tool to capture hourly variations in  $^{222}\text{Rn}$  activity as well as episodic events that might otherwise  
493 be missed if solely relying on discrete  $^{222}\text{Rn}$  measurements. Additionally, the detection limit and  
494 measurement uncertainty using the water probe extraction method (Section 2.3) is much lower  
495 than discrete sampling (Supplementary Material, Figure S1). Our results demonstrate that there is  
496 great potential for continuous  $^{222}\text{Rn}$  measurements in proglacial rivers to aid our understanding  
497 of how distributed system fluxes impact glacial hydrology, ice-dynamics, and biogeochemical  
498 fluxes.

499

500

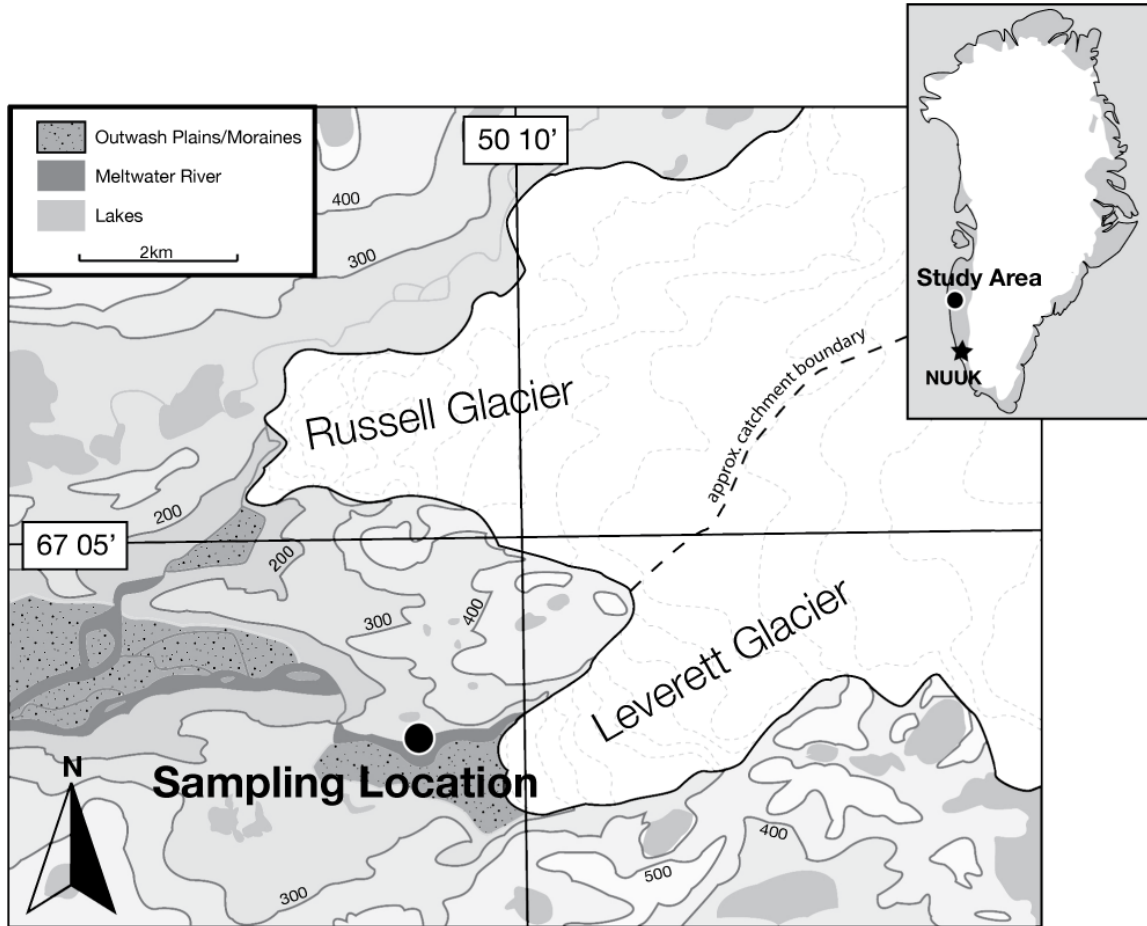
## 501 **Acknowledgements**

502 We acknowledge and thank our funding sources: U.S. National Science Foundation Arctic  
503 Natural Sciences Program (ANS-1256669); Woods Hole Oceanographic Institution Arctic

504 Research Initiative, Ocean Ventures Fund, and Ocean Climate Change Institute; United  
505 Kingdom Natural Environment Research Council studentship (NE/152830X/1); the Carnegie  
506 Trust, Edinburgh University Development Trust. We also thank the Leverett field camp members  
507 who helped with data collection especially Catie Butler for collecting the 2011 electrical  
508 conductivity data that appears in this work. Data presented in this study is archived at:  
509 [www.aoncadis.org/dataset/GrIS\\_RADON.html](http://www.aoncadis.org/dataset/GrIS_RADON.html). Finally, we thank the Editor Derek Vance and  
510 three anonymous reviewers whose suggestions significantly improved this manuscript.  
511



512

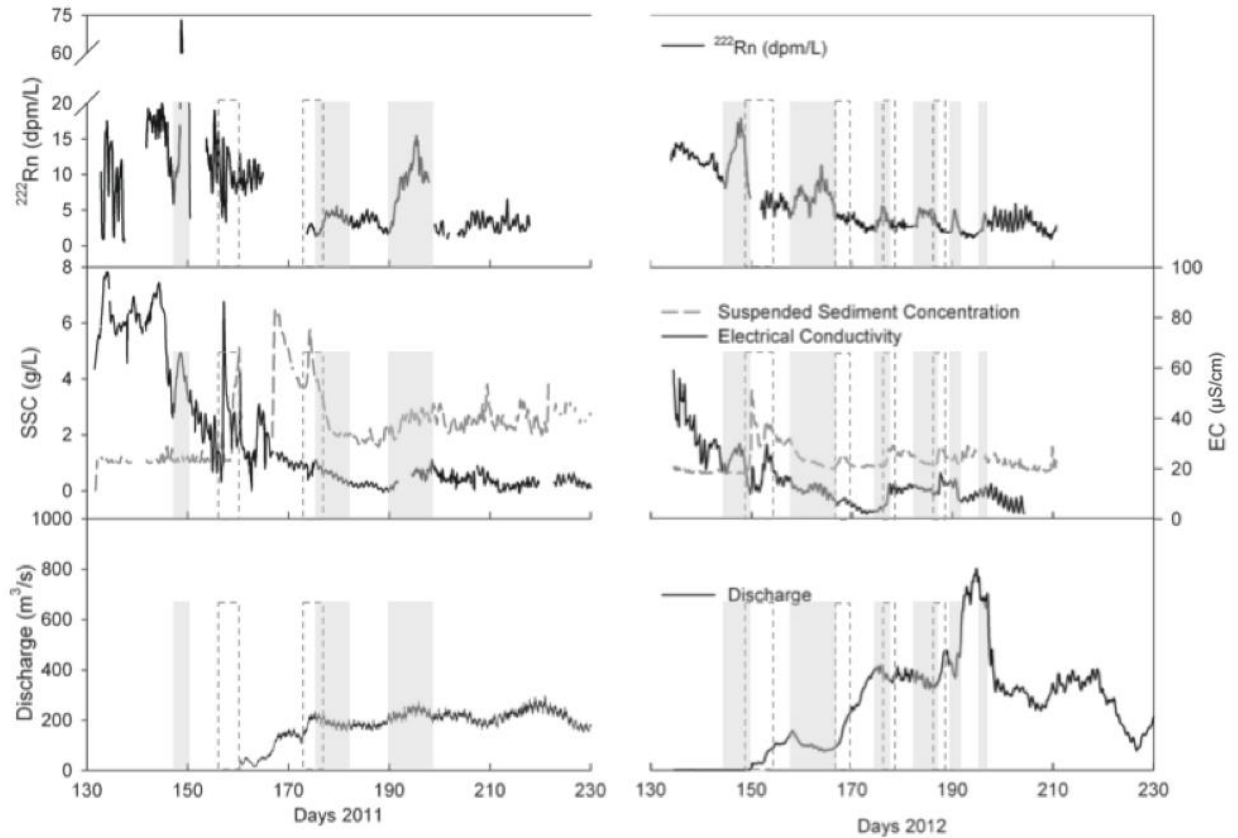


513

514

515 Figure 1: Location of Leverett Glacier in west Greenland. The primary sampling location for  
516 continuous  $^{222}\text{Rn}$  measurements is indicated by the black circle though some early season  
517 deployments of the  $^{222}\text{Rn}$  sensor occurred much closer to the glacier terminus. Figure adapted  
518 from Hawkings et al. (2014).

519

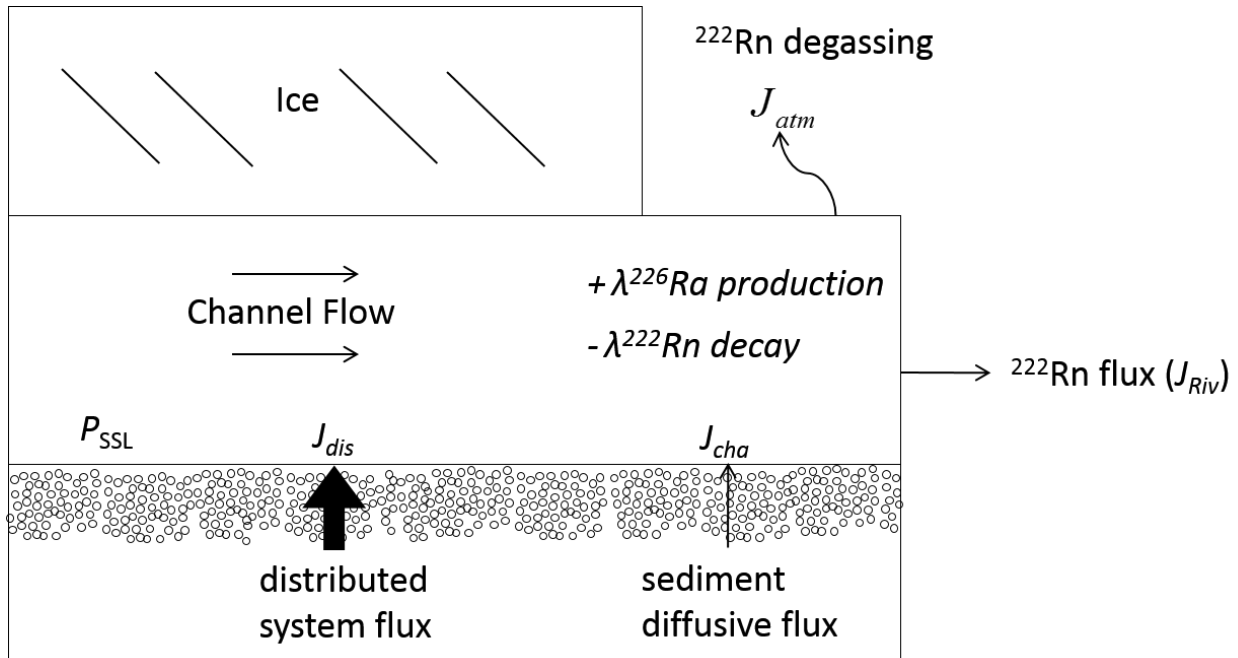


520

521 Figure 2: Results from 2011 and 2012 field seasons. Top panels: radon-222 activity ( $\text{dpm L}^{-1}$ );  
 522 middle panels: EC and SSC (Hawkings et al., 2014); bottom panels: river discharge (Sole et al.,  
 523 2013; Tedstone et al., 2013). Shaded grey boxes represent  $^{222}\text{Rn}$  peaks while dashed grey boxes  
 524 are SSC/EC peaks, which likely correspond to supraglacial lake drainage events (discussed in  
 525 text).

526

527



528

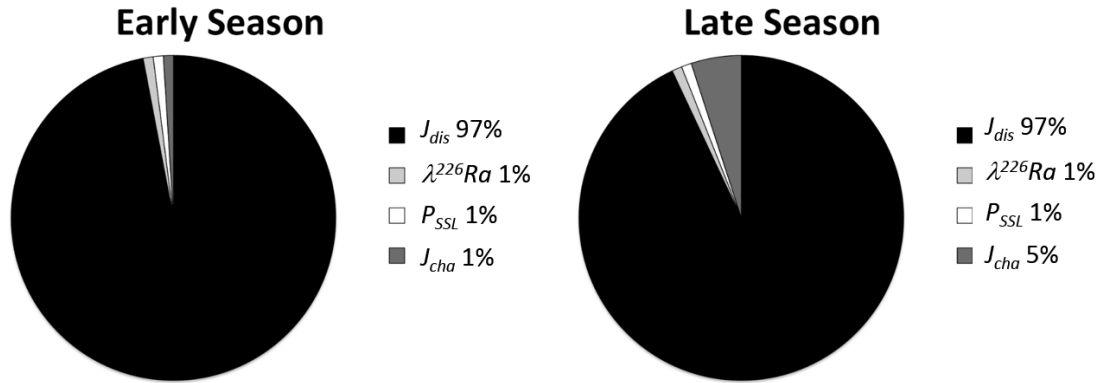
529 Figure 3: Summary of  $^{222}\text{Rn}$  sources and sinks in the proglacial river. Sources of  $^{222}\text{Rn}$  include  
530 the distributed system flux ( $J_{dis}$ ),  $^{222}\text{Rn}$  diffusion through sediments into channels and cavities  
531 ( $J_{cha}$ ),  $^{226}\text{Ra}$  bound to the surface of the suspended sediment load ( $P_{SSL}$ ), and the decay of  
532 dissolved  $^{226}\text{Ra}$  ( $\lambda^{226}\text{Ra}$ ). The sinks of  $^{222}\text{Rn}$  include gas loss to the atmosphere ( $J_{atm}$ ) and  
533 radioactive decay of  $^{222}\text{Rn}$  ( $\lambda^{222}\text{Rn}$ ). The flux of  $^{222}\text{Rn}$  from the river ( $J_{riv}$ ) is the summation of  
534 these variables.

535

536

537

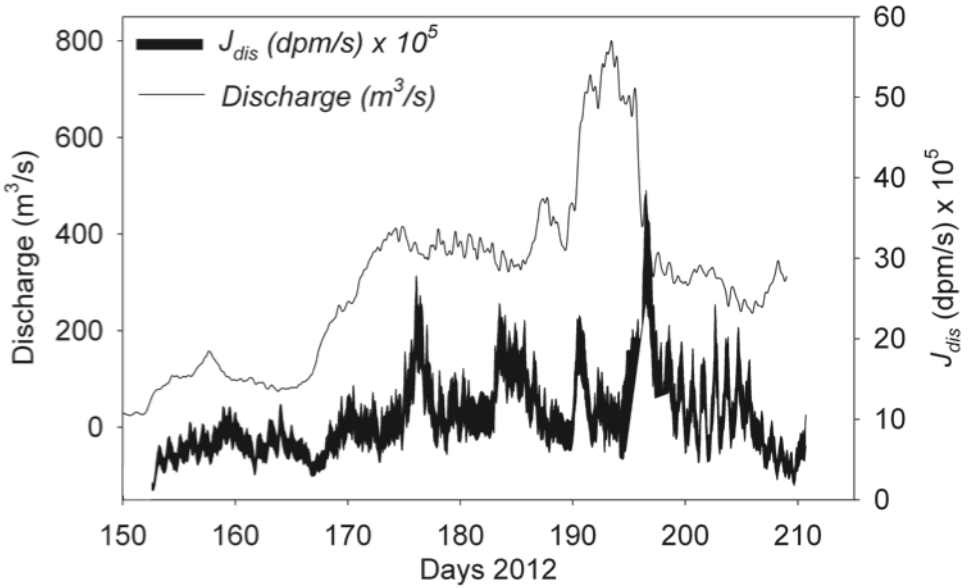
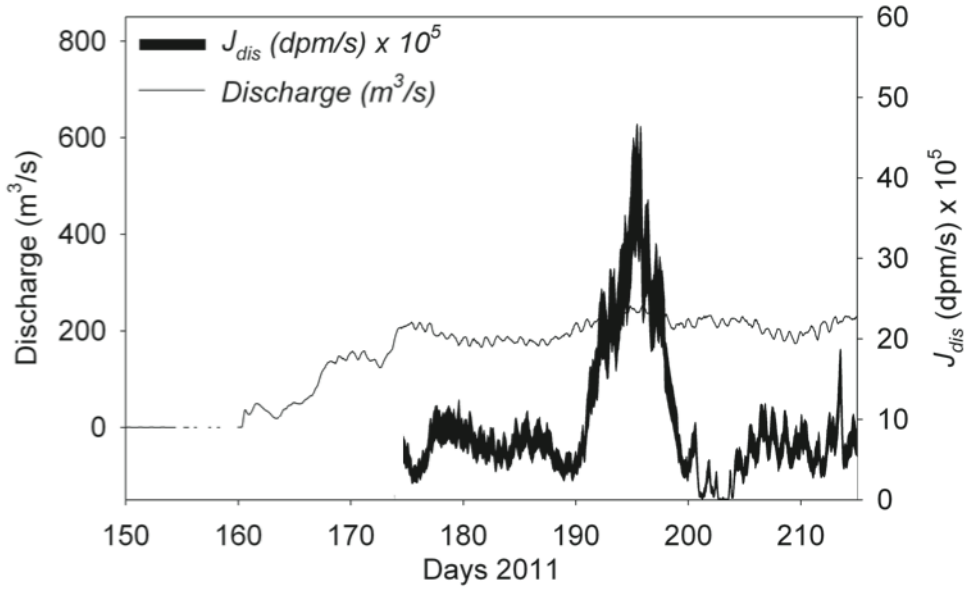
538



539

540 Figure 4: Average contributions from 2011 and 2012 of  $^{222}\text{Rn}$  sources to  $J_{riv}$  in the early melt  
541 season (river discharge  $<100 \text{ m}^3 \text{ s}^{-1}$ ) and during the late melt season (river discharge  $>100 \text{ m}^3 \text{ s}^{-1}$ ). Our mass-balance model suggests that throughout the melt season, the bulk of  $^{222}\text{Rn}$  in the  
542 proglacial river is derived from the distributed system. Model calculations suggested that the  
543  $^{222}\text{Rn}$  contribution from  $P_{SSL}$ ,  $\lambda^{226}\text{Ra}$ , and  $J_{cha}$  were often  $\ll 1\%$  of the total  $J_{riv}$ ; in these  
544 instances, for the purpose of clarity in this figure, they have been rounded to their upper limit  
545 estimates (1%).

547

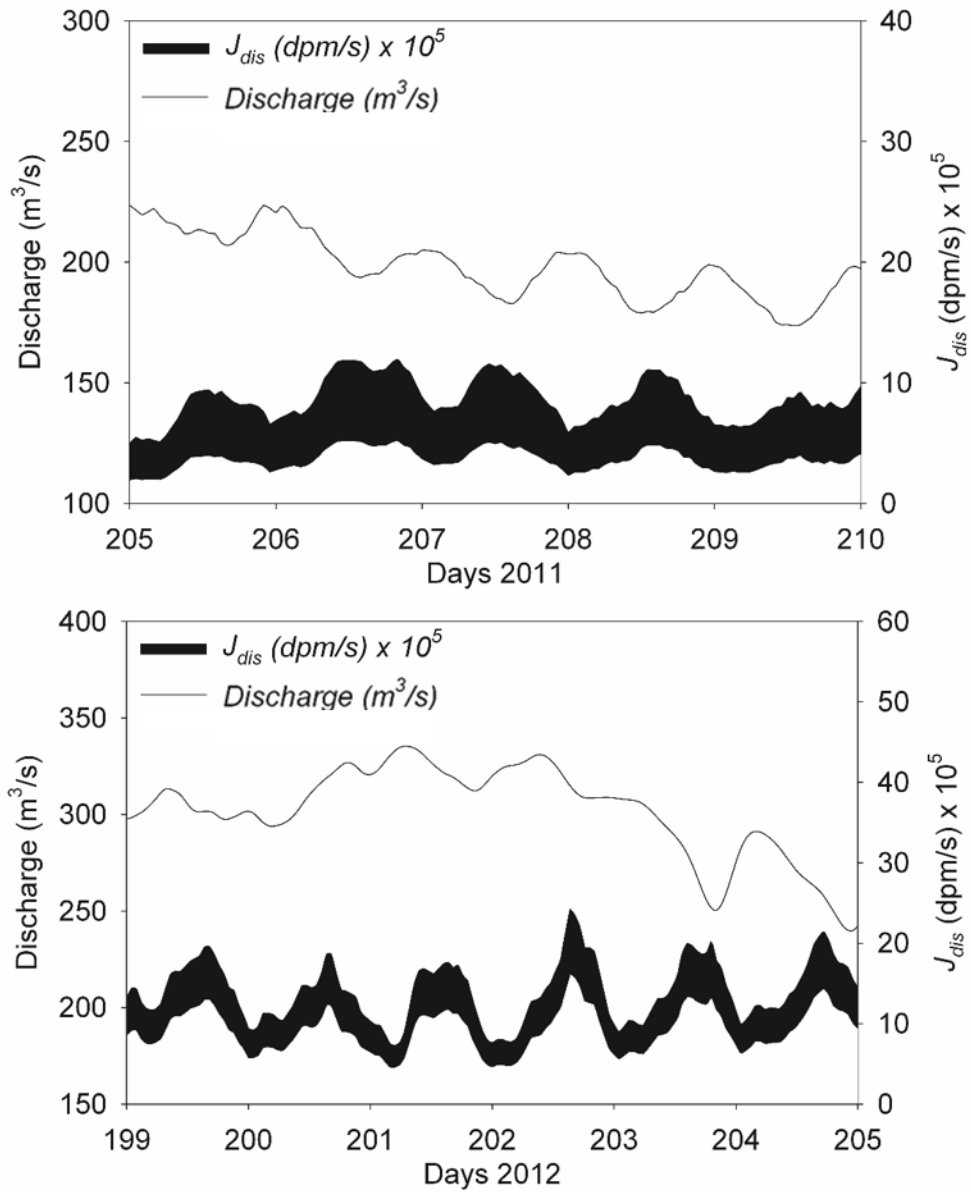


548

549 Figure 5: The estimated subglacial distributed system flux ( $J_{dis}$ ) from Leverett Glacier and  
 550 discharge of the proglacial river in 2011 and 2012 (black line). The width of  $J_{dis}$  represents  
 551 uncertainty in this parameter (see text).

552

553



554

555 Figure 6: Diurnal variations in  $J_{dis}$  occurred in both the 2011 and 2012 melt seasons. In general,  
 556  $J_{dis}$  peaks occurred on the falling limb of the hydrograph. We hypothesize that during this period,

557 distributed system meltwater was drawn into the channelized system as water pressure dropped  
558 in subglacial channels.

559 **Supplementary Material**

560 *S1 Water probe response time*

561 During the 2011 and 2012 field seasons, several factors related to the water probe  
562 setup may have influenced the response time of the water probe. First, in order to keep  
563 the RAD7 a safe distance from the unstable riverbank, the length of tubing between the  
564 detector and water probe had to be increased (from 8 to 12.5 m) effectively changing the  
565 system air volume from 1650 to 1750 cm<sup>3</sup>. Furthermore, the interface area of the  
566 membrane coil changed as two Accruel® membrane coils of slightly different lengths (a  
567 2.1 m coil and the 2.2 m coil within the Durrige Inc. ‘water probe’) were used  
568 interchangeably across the two field seasons. The effect of these changes was quantified  
569 using the empirical relationships developed by Shubert et al., (2012), which suggest that  
570 our minor changes in air volume and membrane interface area likely only caused a 12-  
571 minute difference in equilibration time. This is a negligible difference when considering  
572 that the minimum time-scale over which significant changes in observed river <sup>222</sup>Rn were  
573 diurnal. Furthermore, a field test was conducted in which both membrane coils were  
574 simultaneously deployed in the proglacial river for 12 hours. During this test, both  
575 systems recorded <sup>222</sup>Rn activities well within the statistical counting errors.  
576 Consequently, the continuous <sup>222</sup>Rn record reported here is a compilation of results  
577 obtained using both water probes. During deployment, the membrane coil was checked  
578 daily for wear and sediment buildup on its surface. Throughout either field seasons, no  
579 algae or sediment buildup was observed. To test the effectiveness of long term  
580 deployment of the membrane coil over the course of a melt season, two probes were  
581 deployed simultaneously, one that had been in continual use for ~30 days and a second



582 unit with a new membrane coil. Following an initial equilibration period, both units  
583 measured identical  $^{222}\text{Rn}$  activities (within the method's uncertainty) for several days.

584 To assess the water probe's response to changes in  $^{222}\text{Rn}$  activity, we conducted  
585 several laboratory experiments. First, the water probe was deployed simultaneously with  
586 the more conventional air-water equilibrating spray chamber (Burnett and Dulaiova,  
587 2003) in a 200 L tank of circulating  $10^\circ\text{C}$  seawater for 70 hours. Seawater was  
588 continuously pumped into the tank from Vineyard Sound,  $\sim 50$  m offshore of Woods Hole  
589 (MA). The air-water equilibrator spray chamber provided a baseline from which to  
590 compare the water probe, because with an optimum setup, its equilibration time is less  
591 than 30 minutes (Schubert et al., 2012). The residence time of seawater in the tank was  
592  $<1$  hour and water was kept in constant motion using six submersible bilge pumps, each  
593 capable of pumping  $\sim 30$  L  $\text{min}^{-1}$ . Slow but significant changes in  $^{222}\text{Rn}$  were observed by  
594 both the spray chamber and water probe likely caused by the changing tide and submarine  
595 groundwater discharge (Burnett and Dulaiova, 2003). The equilibration time was defined  
596 as the length of time at which the recorded  $^{222}\text{Rn}$  activities reached an activity plateau  
597 within the statistical counting errors. With this experimental setup, the water probe  
598 required an initial six-hour equilibration time while the spray chamber reached  
599 equilibrium in  $<30$  min. Subsequent changes in  $^{222}\text{Rn}$  activity measured by the water  
600 probe lagged 1-2 hours behind the spray chamber. In a separate experiment, the water  
601 probe and spray chamber were allowed to equilibrate with  $^{222}\text{Rn}$ -free water before being  
602 moved quickly into a tank containing  $^{222}\text{Rn}$ -enriched groundwater. In this case, both  
603 water probe and spray chamber systems responded to the activity change in  $<30$  minutes  
604 though the water probe required much longer to reach the new equilibrium plateau.

605 To determine the equilibration time of the water probe system in the proglacial  
606 river, we examined the first six hours of data recorded after the water probe was freshly  
607 deployed (see Figure S2 for one example). Our analysis included 14 separate  
608 deployments in 2011 and 2012 in river flows ranging from 1 to 750 m<sup>3</sup> s<sup>-1</sup>. In each case,  
609 an equilibration plateau was reached within two hours of deployment regardless of river  
610 flow rate or system configuration (as described above). The equilibration time was  
611 therefore three times faster than the laboratory experiments. This was likely because  
612 water in the proglacial river was flowing much faster than in laboratory experiments  
613 keeping the <sup>222</sup>Rn activity gradient at the water/air interface of the membrane coil closer  
614 to 100%. These results support the findings of Hofmann et al. (2011) and Schubert et al.  
615 (2012) showing that the water flow rate over the membrane coil is the most important  
616 factor for passive <sup>222</sup>Rn extraction. Because of the much faster equilibration time in the  
617 proglacial river, we expect the water probe's response time to changing <sup>222</sup>Rn activities  
618 was also faster in the field than the one to two hours suggested by laboratory  
619 experiments.

620 In summary, when interpreting results from continuous <sup>222</sup>Rn measurements, we  
621 assume changes in <sup>222</sup>Rn activity recorded by our methods occurred within one hour of  
622 actual <sup>222</sup>Rn activity changes in the proglacial river. Also, we have excluded <sup>222</sup>Rn results  
623 from the first two hours from each fresh deployment while the water probe was  
624 equilibrating.

## 625 S2 *Sediment Properties*

626 The porosity and bulk density of glacial flour collected in the proglacial river was

627 determined using the moisture content and particle density measured in the laboratory.  
628 Moisture content (%M) was determined by weighing sediments before and after drying at  
629 100°C: using Equation S1:

630

$$\%M = \frac{\text{wet wt.} - \text{dry wt.}}{\text{wet wt.}} \cdot 100 \quad (\text{S1})$$

631

632

633 Grain density ( $\rho_s$ ) was determined using the oven dry weight and volume of sediment.

634

635 The volume of sediment was determined by adding the sediments to a volumetric flask  
636 and measuring the weight of water displaced by the sediments.

637

638 Bulk density ( $\beta_D$ ) was calculated using Equation S2

639

$$\beta_D = \frac{1}{\left(\left[\frac{1}{100 - \%M}\right] \times 100 + \frac{1}{\rho_z}\right) - 1} \quad (\text{S2})$$

640

641 where  $\rho_s$  is the average sediment grain density of triplicate analysis. Finally, porosity ( $\phi$ )

642

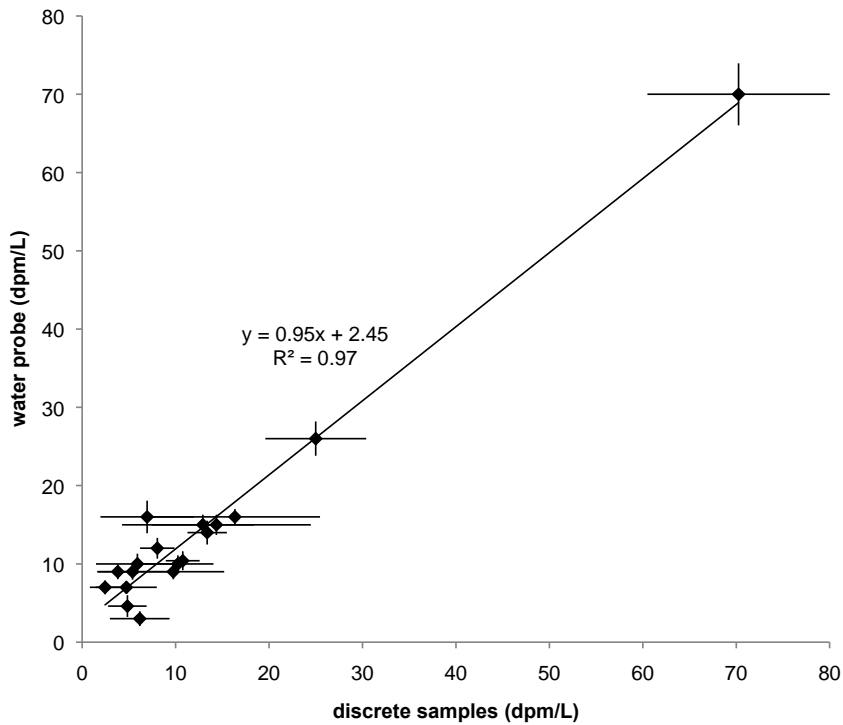
643 was estimated from Equation S3.

644

$$f = (r_s - b_D) / r_s \quad (\text{S3}).$$

645

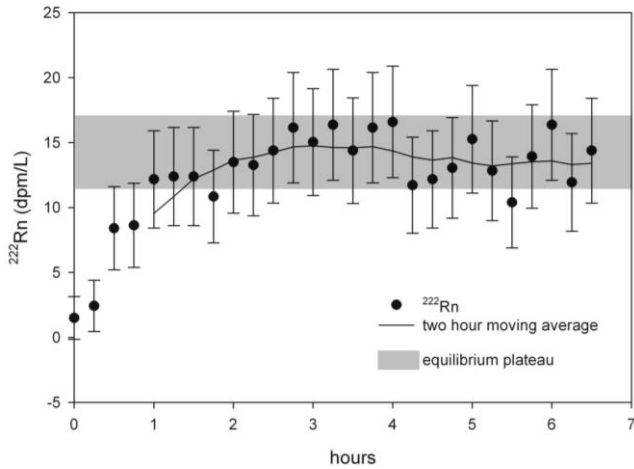




643

644 Figure S1: Comparison of discrete  $^{222}\text{Rn}$  samples with comparable time-series  
 645 measurements using the water probe. Error bars represent 1-sigma counting errors on  
 646 each measurement. Many of these discrete  $^{222}\text{Rn}$  samples were taken at the ice terminus  
 647 while the water probe measured  $^{222}\text{Rn}$  downstream. This implies that gas loss in the  
 648 proglacial river between the ice terminus and the water probe was within the errors of our  
 649 measurements.

650



651

652 Figure S2: Equilibration time of the  $^{222}\text{Rn}$  water probe on 6/2/2011 (day 153) after being  
 653 deployed in the proglacial river. Throughout the 2011 and 2012 field seasons, the water  
 654 probed required 1-2 hours to reach an equilibrium plateau, the time at which the recorded  
 655 radon activities reach an equilibrium activity plateau within the statistical counting errors.

656

657 **Table S1.** Summary of 250 mL discrete  $^{222}\text{Rn}$  samples collected in the proglacial river in  
 658 2011.

Distance	Day	Date	$^{222}\text{Rn}$ dpm L <sup>-1</sup>	+/-	EC $\mu\text{S cm}^{-1}$
0.5	128.5	5/8/11	15.9	6.4	
0.5	129.6	5/9/11	3.2	2.1	
0.5	132.5	5/12/11	3.2	2.8	69
0.5	132.5	5/12/11	7.0	5.4	69
0.5	132.8	5/12/11	4.3	3.0	75
0.5	132.8	5/12/11	5.9	4.4	75
0.5	133.4	5/13/11	4.8	2.1	94
0.5	133.4	5/13/11	7.0	6.4	94
0.5	133.7	5/13/11	18.2	10.1	79
0.5	133.7	5/13/11	14.5	7.5	89
0	133.6	5/13/11	4.3	3.9	
0	133.6	5/13/11	13.4	2.1	
0.5	134.5	5/14/11	9.1	2.1	90
0.5	134.5	5/14/11	7.0	4.4	90
0.5	135.5	5/15/11	5.4	2.8	74
0.5	135.5	5/15/11	7.0	6.2	76
0.5	136.0	5/16/11	10.8	1.8	81
0.5	137.5	5/17/11	9.1	6.2	76
0.5	137.5	5/17/11	1.6	2.0	76
0.5	139.6	5/19/11	4.3	1.8	81
0.5	140.8	5/20/11	5.9	1.1	73
0.5	140.8	5/20/11	5.4	2.8	73
0.5	141.6	5/21/11	14.0	4.1	75
0.5	145.8	5/25/11	4.3	4.7	65
0.5	144.6	5/24/11	6.9	3.2	88
0	147.7	5/27/11	67.4	11.6	49
0	147.7	5/27/11	32.2	7.3	45
0.5	147.8	5/27/11	7.5	2.8	45
0.5	147.8	5/27/11	12.9	3.0	45
0	148.5	5/28/11	41.4	8.1	85
0	148.5	5/28/11	54.3	7.3	84
0.5	148.5	5/28/11	70.3	9.7	62
0.5	149.8	5/29/11	24.3	6.2	40
0	149.8	5/29/11	17.8	8.8	40
0	151.9	5/31/11	17.8	3.1	37
0	148.8	5/28/11	6.5	3.5	61
0	150.8	5/30/11	5.4	1.3	40
0.5	150.8	5/30/11	14.7	6.8	40





Distance	Day	Date	<sup>222</sup> Rn	+/-	EC
			dpm L <sup>-1</sup>		μS cm <sup>-1</sup>
0.5	153.7	6/2/11	22.6	9.5	36
0	153.7	6/2/11	3.2	2.8	36
0	152.7	6/1/11	24.1	7.0	36
0.5	156.6	6/5/11	5.4	3.7	14
0.5	156.6	6/5/11	4.1	4.8	15
0.5	156.7	6/5/11	17.1	3.0	12
0.5	156.7	6/5/11	17.2	5.3	12
0	157.7	6/6/11	4.3	3.0	44
0	157.7	6/6/11	6.5	5.3	45
0.5	158.3	6/7/11	4.8	3.1	21
0.5	159.2	6/8/11	3.8	2.1	37
0.5	159.3	6/8/11	9.7	5.4	36
0.5	153.7	6/2/11	8.2	5.7	42
0.5	153.7	6/2/11	20.5	5.5	50
0.5	162.7	6/11/11	1.6	1.1	16
0.5	162.7	6/11/11	3.3	1.2	16
0.5	165.0	6/14/11	4.9	6.9	35
0.5	165.5	6/14/11	5.4	2.1	27
0	166.7	6/15/11	3.2	2.1	23
0	166.7	6/15/11	10.7	5.8	23
0.5	167.5	6/16/11	2.7	1.1	18
1	167.6	6/16/11	2.7	3.2	18
1	170.0	6/19/11	3.8	1.1	12
1	170.0	6/19/11	4.3	1.8	12
0	172.7	6/21/11	2.7	2.7	14
0	172.7	6/21/11	4.8	4.7	14
0	184.6	7/3/11	2.1	0.9	
1	198.9	7/17/11	1.6	2.0	

660

661

662 **References**

- 663 Andrews, L.C., Catania, G.A., Hoffman, M.J., Gulley, J.D., Luthi, M.P., Ryser, C.,  
664 Hawley, R.L., Neumann, T.A., 2014. Direct observations of evolving subglacial  
665 drainage beneath the Greenland Ice Sheet. *Nature* 514, 80–83.
- 666 Bartholomew, I., Nienow, P., Sole, A., Mair, D., Cowton, T., King, M.A., 2012. Short-  
667 term variability in Greenland Ice Sheet motion forced by time-varying meltwater  
668 drainage: Implications for the relationship between subglacial drainage system  
669 behavior and ice velocity. *J. Geophys. Res. Earth Surf.* 117.  
670 doi:10.1029/2011JF002220
- 671 Bartholomew, I., Nienow, P., Sole, A., Mair, D., Cowton, T., Palmer, S., Wadham, J.,  
672 2011a. Supraglacial forcing of subglacial drainage in the ablation zone of the  
673 Greenland ice sheet. *Geophys. Res. Lett.* 38. doi:10.1029/2011GL047063
- 674 Bartholomew, I.D., Nienow, P., Sole, A., Mair, D., Cowton, T., King, M.A., Palmer, S.,  
675 2011b. Seasonal variations in Greenland Ice Sheet motion: Inland extent and  
676 behavior at higher elevations. *Earth Planet. Sci. Lett.* 307, 271–278.
- 677 Bhatia, M.P., Das, S.B., Kujawinski, E.B., Henderson, P., Burke, A., Charette, M.A.,  
678 2011. Seasonal evolution of water contributions to discharge from a Greenland  
679 outlet glacier: insight from a new isotope-mixing model. *J. Glaciol.* 57, 929–941.

680 Borges, A.V., Vanderborcht, J.-P., Schiettecatte, L.-S., Gazeau, F., Ferrón-Smith, S.,  
681 Delille, B., Frankignoulle, M., 2004. Variability of the gas transfer velocity of CO<sub>2</sub>  
682 in a macrotidal estuary (the Scheldt). *Estuaries* 27, 593–603.

683 Boulton, G.S., Hagdorn, M., Maillot, P.B., Zatsepin, S., 2009. Drainage beneath ice  
684 sheets: groundwater–channel coupling, and the origin of esker systems from former  
685 ice sheets. *Quat. Sci. Rev.* 28, 621–638.

686 Burnett, W.C., Dulaiova, H., 2003. Estimating the dynamics of groundwater input into  
687 the coastal zone via continuous radon-222 measurements. *J. Environ. Radioact.* 69,  
688 21–35.

689 Chandler, D.M., Wadham, J.L., Lis, G.P., Cowton, T., Sole, A., Bartholomew, I., Telling,  
690 J., Nienow, P., Bagshaw, E.B., Mair, D., 2013. Evolution of the subglacial drainage  
691 system beneath the Greenland Ice Sheet revealed by tracers. *Nat. Geosci.* 6, 195–  
692 198.

693 Chandler, D.M., Wadham, J.L., Nienow, P.W., Hawkings, J., Doyle, S.H., Telling, J.,  
694 Tedstone, A., Hubbard, A., Rapid growth and persistence of efficient subglacial  
695 drainage under kilometre thick Greenland ice. Submitted.

696 Chanyotha, S., Kranrod, C., Burnett, W.C., 2014. Assessing diffusive fluxes and pore  
697 water radon activities via a single automated experiment. *J. Radioanal. Nucl. Chem.*  
698 1–8.

699 Charette, M.A., Buesseler, K.O., Andrews, J.E., 2001. Utility of radium isotopes for  
700 evaluating the input and transport of groundwater-derived nitrogen to a Cape Cod  
701 estuary. *Limnol. Oceanogr.* 46, 465–470.

702 Charette, M.A., Moore, W.S., Burnett, W.C., 2008. Uranium-and thorium-series nuclides  
703 as tracers of submarine groundwater discharge. *U-Th Ser. nuclides Aquat. Syst.*  
704 Elsevier 155–191.

705 Collins, D.N., 1979. Hydrochemistry of meltwaters draining from an alpine glacier. *Arct.*  
706 *Alp. Res.* 307–324.

707 Cook, P.G., Favreau, G., Dighton, J.C., Tickell, S., 2003. Determining natural  
708 groundwater influx to a tropical river using radon, chlorofluorocarbons and ionic  
709 environmental tracers. *J. Hydrol.* 277, 74–88.

710 Corbett, D.R., Burnett, W.C., Cable, P.H., Clark, S.B., 1998. A multiple approach to the  
711 determination of radon fluxes from sediments. *J. Radioanal. Nucl. Chem.* 236, 247–  
712 253.

713 Cowton, T., Nienow, P., Bartholomew, I., Sole, A., Mair, D., 2012. Rapid erosion  
714 beneath the Greenland ice sheet. *Geology* 40, 343–346.

715 Cowton, T., Nienow, P., Sole, A., Wadham, J., Lis, G., Bartholomew, I., Mair, D.,  
716 Chandler, D., 2013. Evolution of drainage system morphology at a land-terminating  
717 Greenlandic outlet glacier. *J. Geophys. Res. Earth Surf.* 118, 29–41.

718 Creyts, T.T., Schoof, C.G., 2009. Drainage through subglacial water sheets. *J. Geophys.*  
719 *Res. Earth Surf.* 114.

720 Das, S.B., Joughin, I., Behn, M.D., Howat, I.M., King, M. a, Lizarralde, D., Bhatia, M.P.,  
721 2008. Fracture propagation to the base of the Greenland Ice Sheet during  
722 supraglacial lake drainage. *Science* 320, 778–81. doi:10.1126/science.1153360

723 Dow, C.F., Hubbard, A., Booth, A.D., Doyle, S.H., Gusmeroli, A., Kulesa, B., 2013.  
724 Seismic evidence of mechanically weak sediments underlying Russell Glacier, West  
725 Greenland. *Ann. Glaciol.* 54, 135–141. doi:10.3189/2013AoG64A032

726 Dulaiova, H., Burnett, W.C., 2006. Radon loss across the water-air interface (Gulf of  
727 Thailand) estimated experimentally from  $^{222}\text{Rn}$ - $^{224}\text{Ra}$ . *Geophys. Res. Lett.* 33.  
728 doi:10.1029/2005GL025023

729 Dulaiova, H., Gonnee, M.E., Henderson, P.B., Charette, M.A., 2008. Geochemical and  
730 physical sources of radon variation in a subterranean estuary—implications for  
731 groundwater radon activities in submarine groundwater discharge studies. *Mar.*  
732 *Chem.* 110, 120–127.

733 Gonnee, M.E., Morris, P.J., Dulaiova, H., Charette, M.A., 2008. New perspectives on  
734 radium behavior within a subterranean estuary. *Mar. Chem.* 109, 250–267.

735 Gulley, J.D., Benn, D.I., Screatton, E., Martin, J., 2009. Mechanisms of englacial conduit  
736 formation and their implications for subglacial recharge. *Quat. Sci. Rev.* 28, 1984–  
737 1999.

- 738 Hawkings, J.R., Wadham, J.L., Tranter, M., Raiswell, R., Benning, L.G., Statham, P.J.,  
739 Tedstone, A., Nienow, P., Lee, K., Telling, J., 2014. Ice sheets as a significant  
740 source of highly reactive nanoparticulate iron to the oceans. *Nat. Commun.* 5.  
741 doi:10.1038/ncomms4929
- 742 Henriksen, N., Higgins, A.K., Kalsbeek, F., Pulvertaft, T.C.R., 2009. Greenland from  
743 Archaean to Quaternary: descriptive text to the 1995 geological map of Greenland,  
744 1: 2 500 000. Geological Survey of Denmark and Greenland.
- 745 Hindshaw, R.S., Rickli, J., Leuthold, J., Wadham, J., Bourdon, B., 2014. Identifying  
746 weathering sources and processes in an outlet glacier of the Greenland Ice Sheet  
747 using Ca and Sr isotope ratios. *Geochim. Cosmochim. Acta* 145, 50–71.
- 748 Hofmann, H., Gilfedder, B.S., Cartwright, I., 2011. A novel method using a silicone  
749 diffusion membrane for continuous  $^{222}\text{Rn}$  measurements for the quantification of  
750 groundwater discharge to streams and rivers. *Environ. Sci. Technol.* 45, 8915–8921.
- 751 Hubbard, B., Sharp, M., Nielsen, M., Willis, I.C., Smart, C.C., 1995. Borehole water-  
752 level variations and the structure of the subglacial hydrological system of Haut  
753 Glacier d' Rolla, Valais, Switzerland. *J. Glaciol.* 41, 572–583.
- 754 Kies, A., Nawrot, A., Tosheva, Z., Jania, J., 2011. Natural radioactive isotopes in glacier  
755 meltwater studies. *Geochem. J.* 45, 423–429.

756 Kies, a., Henges, O., Tosheva, Z., Nawrot, a. P., Jania, J., 2015. Overview on radon  
757 measurements in Arctic glacier waters. *Cryosph. Discuss.* 9, 2013–2052.  
758 doi:10.5194/tcd-9-2013-2015

759 McCallum, J.L., Cook, P.G., Berhane, D., Rumpf, C., McMahon, G.A., 2012.  
760 Quantifying groundwater flows to streams using differential flow gaugings and  
761 water chemistry. *J. Hydrol.* 416, 118–132.

762 Meierbachtol, T., Harper, J., Humphrey, N., 2013. Basal drainage system response to  
763 increasing surface melt on the Greenland Ice Sheet. *Science* 341, 777–779.

764 Nghiem, S. V, Hall, D.K., Mote, T.L., Tedesco, M., Albert, M.R., Keegan, K., Shuman,  
765 C.A., DiGirolamo, N.E., Neumann, G., 2012. The extreme melt across the  
766 Greenland ice sheet in 2012. *Geophys. Res. Lett.* 39.

767 Niu, Y., Clara Castro, M., Aciego, S.M., Hall, C.M., Stevenson, E.I., Arendt, C.A., Das,  
768 S.B., 2015. Noble gas signatures in Greenland: Tracing glacial meltwater sources.  
769 *Geophys. Res. Lett.* 42, 9311–9318. doi:10.1002/2015GL065778

770 Nye, J.F., 1973. Water at the bed of a glacier, in: *International Association of Scientific*  
771 *Hydrologists Publication*, 95. pp. 189–194.

772 Raiswell, R., 1984. Chemical models of solute acquisition in glacial meltwaters. *J.*  
773 *Glaciol.* 30, 49–57.

774 Rempel, A.W., 2009. Transient effective stress variations forced by changes in conduit  
775 pressure beneath glaciers and ice sheets. *Ann. Glaciol.* 50, 61–66.



776 Röthlisberger, H., 1972. Water Pressure in Intra-and Subglacial Channels: Pres. at the  
777 Symposium on the Hydrology of Glaciers, 7-13 September 1969, Cambridge.

778 Schoof, C., 2010. Ice-sheet acceleration driven by melt supply variability. *Nature* 468,  
779 803–806.

780 Schubert, M., Paschke, A., Bednorz, D., Bürkin, W., Stieglitz, T., 2012. Kinetics of the  
781 water/air phase transition of radon and its implication on detection of radon-in-water  
782 concentrations: practical assessment of different on-site radon extraction methods.  
783 *Environ. Sci. Technol.* 46, 8945–8951.

784 Sharp, M., Richards, K., Willis, I., Arnold, N., Nienow, P., Lawson, W., Tison, J., 1993.  
785 Geometry, bed topography and drainage system structure of the Haut Glacier  
786 d’Arolla, Switzerland. *Earth Surf. Process. Landforms* 18, 557–571.

787 Sole, A., Nienow, P., Bartholomew, I., Mair, D., Cowton, T., Tedstone, A., King, M.A.,  
788 2013. Winter motion mediates dynamic response of the Greenland ice sheet to  
789 warmer summers. *Geophys. Res. Lett.* 40, 3940–3944.

790 Tedstone, A.J., Nienow, P.W., Sole, A.J., Mair, D.W.F., Cowton, T.R., Bartholomew,  
791 I.D., King, M.A., 2013. Greenland ice sheet motion insensitive to exceptional  
792 meltwater forcing. *Proc. Natl. Acad. Sci.* 110, 19719–19724.

793 Tranter, M., 1993. A conceptual model of solute acquisition by Alpine glacial  
794 meltwaters. *J. Glaciol.* 39.

- 795 Tranter, M., Sharp, M.J., Brown, G.H., Willis, I.C., Hubbard, B.P., Nielsen, M.K., Smart,  
796 C.C., Gordon, S., Tulley, M., Lamb, H.R., 1997. Variability in the chemical  
797 composition of in situ subglacial meltwaters. *Hydrol. Process.* 11, 59–77.  
798 doi:10.1002/(SICI)1099-1085(199701)11:1<59::AID-HYP403>3.0.CO;2-S
- 799 Walder, J.S., 1986. Hydraulics of subglacial cavities. *J. Glaciol* 32, 439–445.
- 800 Werder, M.A., Hewitt, I.J., Schoof, C.G., Flowers, G.E., 2013. Modeling channelized and  
801 distributed subglacial drainage in two dimensions. *J. Geophys. Res. Earth Surf.* 118,  
802 2140–2158.